

Bistable carbon-vacancy defects in *h*-BN

Song Li

Wigner Research Centre for Physics, P.O. Box 49, H-1525 Budapest, Hungary

Adam Gali

Wigner Research Centre for Physics, P.O. Box 49, H-1525 Budapest, Hungary and

Department of Atomic Physics, Institute of Physics,

Budapest University of Technology and Economics,

Műgyetem rakpart 3., H-1111 Budapest, Hungary

(Dated: September 19, 2022)

Single photon emitters in hexagonal boron nitride have been extensively studied recently. Although unambiguous identification of the emitters is still under intense research, carbon related defects are believed to play a vital role for the emitter producing zero-phonon-lines in the range of 1.6 to 2.2 eV. In this study, we systematically investigate two configurations of carbon-vacancy defects, $V_N C_B$ and $C_N V_B$, by means of density functional theory calculations. We calculated the reaction barrier energies from one defect to the other to determine relative stability. We find the barrier energies are charge dependent and $C_N V_B$ could easily transform to $V_N C_B$ in neutral and positive charge states while it is stable when negatively charged. Formation energy calculations show that the $V_N C_B$ is the dominant defect over $C_N V_B$. However, neither $V_N C_B$ nor $C_N V_B$ has suitable fluorescence spectra that could reproduce the observed ones. Our results indicate that the origin of the 1.6-to-2.2-eV emitters should be other carbon-related configurations.

I. INTRODUCTION

Point defects as emerging single photon emitters (SPEs) in two-dimensional (2D) hexagonal boron nitride (hBN) have been intensively studied for possible applications in quantum sensing, computing and nanophotonics [1–8]. The wide band gap (~ 6 eV) and small spin-orbital coupling of hBN manifests itself as ideal host to accommodate color centers in a wide region of emission wavelength. The spatial confinement and dielectric screening of 2D defects enable them showing desirable properties, for example, bright luminescence, ease of manipulation, tunable emission through strain [5, 9, 10] and electric fields [11] motivating researchers to investigate the underlying physical and chemical nature of the structures in detail. However, direct mapping or characterization of the defects in experiment is still a challenge. This might be partially related to various defect types and unintentional impurities during hBN sample fabrication and post-processing.

Photoluminescence data reveals that there are strong emission bands in ultraviolet region with zero-phonon-line (ZPL) energy at 4.1 eV [6, 12–14] and in visible region from 1.6 to 2.2 eV [1–4, 8, 15, 16]. Based on this, many kinds of point defects have been proposed and analyzed theoretically through density functional theory (DFT) calculations. Several of them could match the experimental result well, such as the boron vacancy (V_B) [17–19], nitrogen vacancy (V_N) [20], and Stone-Wales defect [21, 22]. V_B have been identified experimentally [23–26] and single spins of other defects could be coherently manipulated [3, 27]. Besides, defect complexes and impurities that deliberately incorporated during synthesis or ion implantation also could serve as potential candidates [2–4, 20, 28, 29]. Among them, car-

bon impurity in hBN has been extensively considered and investigated. Previous study indicated that the recombination from C_N as a donor-acceptor pair with V_N donor [13] should not be related to 4.1-eV emission line due to the deep donor level of V_N whereas the C_B might be a possible source with charge transition level (0/+) at 3.71 eV [29]. Later carbon dimer $C_N C_B$ was also associated to this emission with a calculated ZPL at 4.3 eV [30, 31]. For the visible emission, both $V_N C_B$ and $C_N V_B$ are considered depending on their charge states and spin multiplicity. Our study already revealed the positively charged $V_N C_B(+)$ has ZPL about 1.5 eV which could be classified to so called “Group-2” SPE [17]. In the triplet electronic configuration of its neutral charge state, the two defects have ZPL optical transitions at 1.58 eV and 1.54 eV, respectively [20]. A recent study has indicated that the quartet state of the negatively charged $C_N V_B(-)$ is the origin of the SPEs in carbon doped hBN [4].

The robust emission features from carbon defects in hBN samples grown with different techniques and environment indicate that they come from very stable configurations. However, considering the fact that the carbon atom in $V_N C_B$ and $C_N V_B$ structures can migrate easily under external perturbation, it is necessary to investigate the relative stability and transformation of the two defects in detail. Formation energy and energy barrier calculation can help to identify the possible structures. The experimental observed ZPL emission is about 1.6 to 2.2 eV with Huang-Rhys factor less than 2. Here we use these criteria to examine the possibility of $V_N C_B$ and $C_N V_B$ as single photon emitter candidates. In this paper, we employ plane-wave supercell DFT calculations to study the energetic and electronic properties of $V_N C_B$ and $C_N V_B$ at different charge states and spin multiplici-

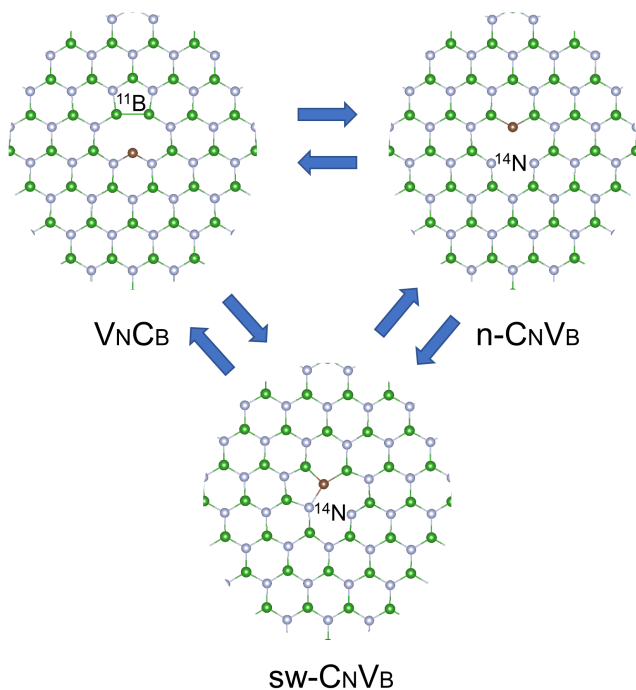


FIG. 1. Schematic view of carbon-vacancy complexes in hBN. The carbon atom can migrate to the antisite-vacancy configuration. Grey, green, and brown colored balls represent nitrogen, boron and carbon atoms, respectively. The usual $C_N V_B$ considered before is denoted as $n-C_N V_B$.

ties. We find that the charge states influence the relative stability of the two proposed defects. Although the ZPL energy of $C_N V_B(-)$ with quartet spin multiplicity is in the experimental range of interest, the calculated formation energy and charge transition level (CTL) indicate that the quartet state is not stable. Our results imply that the charge states of defects can dramatically affect their relative stability and provide further evidence for the identification of quantum emitters in the visible region.

II. RESULTS

The ground state electronic structures are calculated for $V_N C_B$ and $C_N V_B$ in -1 , 0 and $+1$ charged states with the high-spin (HS) and low-spin (LS) states included. Previous results about the spin multiplicity of the ground state varied with the applied calculation methods [4, 20]. For neutral $V_N C_B(0)$, Cheng *et al.* [32] predicted a triplet ground state, however, further comprehensive calculations indicated that the 1A_1 singlet is the most favorable one [33]. Our calculation shows that the singlet (LS) state of $V_N C_B(0)$ has lower energy considering the symmetry reduction caused by the pseudo-Jahn-Teller (JT) distortion in the singlet state while it does not occur in the triplet state. The C_s symmetry configuration is lower in energy by 1.87 eV over that of C_{2v} symmetry configura-

tion. In the following calculation, we remove the symmetry constrain and investigate the electronic structure. We find that the C_{2v} symmetry is the most stable on in the positive charge state regardless the spin multiplicity, and $V_N C_B(+)$ prefers the low-spin doublet (LS). Meanwhile, $V_N C_B(-)$ exhibits doublet state with C_s symmetry.

For the $C_N V_B$ defect ($n-C_N V_B$ in this paper), the triplet state is predicted to have lower energy than singlet for $C_N V_B(0)$ with transition energy in experimental value [20]. However, a recent report indicates that this configuration suffers from multiple low-energy minima, and none of them has significant oscillator strength [4]. Noteworthy, we find that the $C_N V_B$ could form a Stone-Wales-like ($sw-C_N V_B$) configuration, as shown in Fig. 1, which could have lower formation energy. The multireference character still exists here which is manifested as the unrestricted spin-polarized calculation yields different energy for spin-up and spin-down channels. We speculate this phenomenon is due to the spin contamination from the triplet ground state and indeed the calculated energy of the singlet is almost identical to that of the triplet. Although these states are not spin eigenstates, the unrestricted DFT orbitals provide more realistic total energies. Except for HSs of $C_N V_B(-)$, other electronic states prefer the $sw-C_N V_B$ configuration. In the following discussion, always the most stable configuration is discussed for $C_N V_B$ defects in the context. LSs always have lower energy whereas the CCSD methods pointed out the HS quartet for $C_N V_B(-)$ could be the ground state [4]. This controversy motivated us to further investigate the relative stability of carbon impurity in these two defects.

The energy level diagrams for the two defects are shown in Fig. 2. $V_N C_B(-)$ at both HS and LS states do not have empty localized state therefore only defect-to-conduction band (CB) excitation occurs which results in a relatively dim emission. The experimental observed bright luminescence should come from defect states in the fundamental band gap and neither of the vertical transition energies is in line with the experimental PL energies. The $V_N C_B(0)$ HS state with C_{2v} symmetry has been studied [34], the defect demonstrates suitable ZPL energy and 1.5 Huang-Rhys (HR) factor. However, the HR factor of the more stable LS state in C_s is 7.25, much larger than the experimental value 1.45. The ZPL of $V_N C_B(+)$ LS is 1.51 eV [17], which agree relatively well with the experimental data for the Group-2 emitters. Despite of that, the corresponding HR factor is about 24 so we can also disregard as a good candidate for the observed visible emitters. $C_N V_B(-)$ with both HS and LS states have defect-to-defect transitions. The singlet $C_N V_B(0)$ has ZPL of 1.98 eV and we believe this value is still in the range of interest even taking into account the possible error due to multireference character of the ground state, however, the HR factor is 8.17. There are no occupied defect states in the gap for $C_N V_B(+)$ and the allowed transition is between valence band maximum to defect states which should result in again a relatively

dim optical transition.

We summarized the calculated lowest vertical excitation energies in Tab. I. For defects in the negative charge state, the $C_N V_B(-)$ with HS state is the only possible candidate for the bright visible emitters, and the defects in other charge states have either too small transition energy or large phonon side band. The calculated ZPL is 1.89 eV which is close to that obtained in the flake model [4].

The defect formation energies E_f are calculated to determine the charge stability with the following equation,

$$E_f^q = E_d^q - E_{\text{per}} + \mu_C - \mu_B - \mu_N + q(\epsilon_{\text{VBM}}^{\text{per}} + \epsilon_{\text{Fermi}}) + E_{\text{corr}}(q), \quad (1)$$

where E_d^q is the total energy of hBN model with defect at q charge state and E_{per} is the total energy of hBN layer without defect. μ_C is the chemical potential of carbon and can be derived from pure graphite. The Fermi-level ϵ_{Fermi} represents the chemical potential of electron reservoir and it is aligned to the valence band maximum (VBM) energy of perfect hBN, $\epsilon_{\text{VBM}}^{\text{per}}$. The $E_{\text{corr}}(q)$ is the correction term for the charged system due to the existence of electrostatic interactions of the periodic images of the defect. $V_N C_B$ and $C_N V_B$ always prefers LS state for different charge states. As shown in Fig. 3, in the fundamental gap, the CTL of $V_N C_B$ for (+1/0) is 2.88 eV and it is 5.30 eV for (0/-1) with respect to VBM. These CTLs are far from conduction band minimum (CBM) and VBM, respectively, making $V_N C_B$ a hyper deep donor and acceptor. For $C_N V_B$, the (+1/0) and (0/-1) levels are at 1.51 eV and 3.19 eV, respectively. We notice that the +2 charge state of $V_N C_B$ and -2 charge state of $C_N V_B$ are also stable as reported previously [35]. $V_N C_B(+2)$ have C_{2v} symmetry and the $C_N V_B(-2)$ have n- $C_N V_B$ configuration. However, the calculated CTLs are relatively close to the band edge. (+2/+1) is at 1.11 eV for $V_N C_B$ while the (-1/-2) is at 4.49 eV for $C_N V_B$. Optical excitation results in photoionization to other charge states and thus cannot have optical transition energies in fluorescence close to the experimental values. $V_N C_B$ is generally more stable with lower formation energy than $C_N V_B$ when $\epsilon_{\text{Fermi}} < 4.75$ eV. The $C_N V_B(-2)$ has lower formation energy with Fermi-level close to CBM which is not a typical experimental condition.

Next, we calculated the defect migration with the climbing-image nudged-elastic-band method [36, 37] as shown in Fig. 4. The n- $C_N V_B$ and sw- $C_N V_B$ are both considered here. The carbon atom can migrate between boron site and nitrogen site and this transition rate Γ can be simply expressed as [29],

$$\Gamma = \Gamma_0 \exp\left(-\frac{E_b}{k_B T}\right), \quad (2)$$

where E_b is the reaction barrier energy, k_B is the Boltzmann constant, T is the temperature and Γ_0 is typical

phonon frequency in hBN which is about 10^{14}s^{-1} [38]. The calculated T can be regarded as annealing temperature at which the defect becomes mobile as listed in Tab. I. Usually the temperature is estimated when the jump rate Γ is 1/s [39]. Above this temperature, the reaction barrier can be passed to reach an equilibrium point. In the negative charge state, the reaction barrier energies for LSs and HSs are 0.98 eV and 1.96 eV, respectively, for carbon migration from boron site to nitrogen site. The large barrier energies indicate that the carbon atom cannot jump from one site to another, therefore, the two defects could exist simultaneously. The annealing temperature are 353 K and 705 K, therefore, $V_N C_B$ would transform to $C_N V_B$ if the sample is grown or annealed above these temperatures. However, the barrier energies are quite small in the neutral and positive charge states. The barrier energies are generally less than 0.6 eV, especially, for LSs in the neutral state, manifesting the carbon can move freely from nitrogen site to boron site. The calculated annealing temperature is lower than room temperature, hence the $V_N C_B$ defect will dominate in these two charge states, and the $C_N V_B$ can only be stabilized through low-temperature irradiation.

The reaction barrier energies and migration paths depend on the charge state. We tentatively associate the low stability of $C_N V_B(0)$ and $C_N V_B(+)$ to the unoccupied localized states in the gap. Filling these defect levels by electrons could stabilize the defect.

III. DISCUSSION

We calculated the formation energies and the barrier energy of transformation of carbon-vacancy complexes depending on the symmetry and spin multiplicities. We note that the geometry distortions from the planar structure was found for certain carbon-vacancy complexes as the common Jahn-Teller distortion effect where the atoms farther the core of the defect structure remain in the sheet of hBN layer. This is different from recent proposed geometry containing dramatically out-of-plane warping calculated by CAM-B3LYP DFT functional [4]. This warping might be induced by the hydrogen termination of the model or the freezing of atoms during optimization. In addition, the large scale distortion might yield opposite result. In our model, the relaxation energy of HS $C_N V_B(-)$ is 0.16 eV and HR factor is 2.2 which are close to the experimental data [4]. However, the formation energy difference between the HS and LS for n- $C_N V_B(-)$ is 0.4 eV, where the LS configuration exhibits C_{2v} symmetry. Our NEB calculation shows there is no barrier for n- $C_N V_B$ to transform to sw- $C_N V_B$ at LSs for three charge states which indicates the n- $C_N V_B$ might not exist at all. Recent work indicates that n- $C_N V_B$ is dynamically unstable and it quickly relax to $V_N C_B$ defect [40]. This is consistent with our present data for the neutral charge state. We show here that sw- $C_N V_B$ occurs in the other charge states too, thus this behavior is

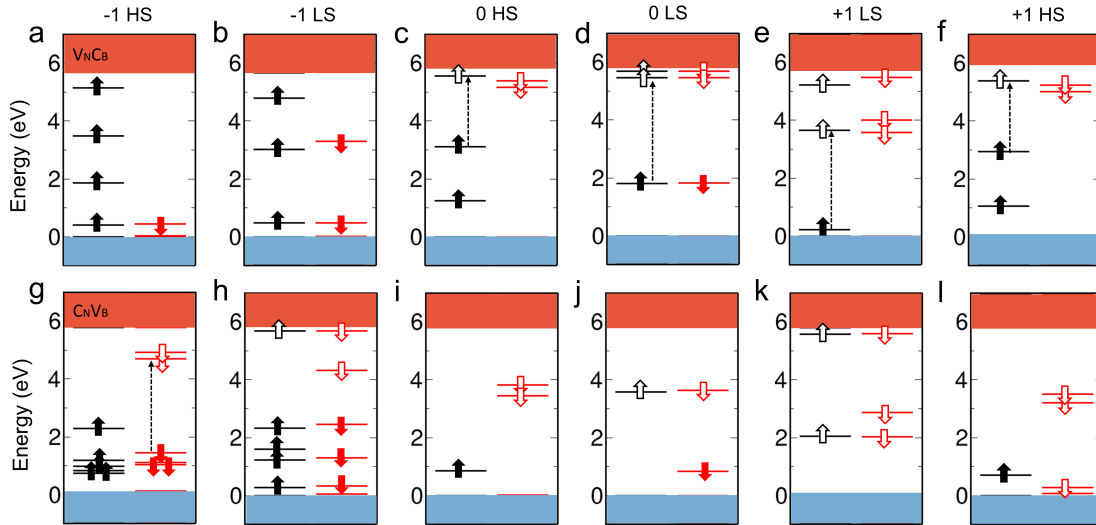


FIG. 2. Energy level diagram of $V_N C_B$ (a-f) and $C_N V_B$ (g-l) with different charge states and spin multiplicities. The filled and empty arrows indicate the occupied and unoccupied defect states in the spin-up and spin-down channels. Resonant defect levels below valence band maximum are not shown here. The dash lines represent the allowed optical transition in the visible wavelength region. We use the most stable configurations at every charge and spin states. Here, the $C_N V_B(-2)$ and HSs of $C_N V_B(-)$ have $n-C_N V_B$ configuration and the others are calculated with $sw-C_N V_B$.

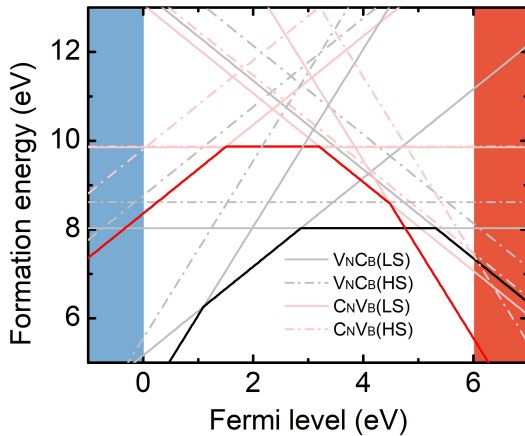


FIG. 3. The formation energies of $V_N C_B$ (black) and $C_N V_B$ (red) as a function of the Fermi-level. The slope of line segment corresponds to the charge state. The solid and dash lines indicate the LS and HS state, respectively. Crossing of the lines denote the charge transition level. Here, the $C_N V_B(-2)$ and HSs of $C_N V_B(-)$ have $n-C_N V_B$ configuration and the others are calculated with $sw-C_N V_B$.

independent on the position of the Fermi-level of hBN.

Similar to V_B [2], hyperfine interaction related features may be a unique fingerprint of the $C_N V_B(-)$ defect observed by electron spin resonance techniques. Recently, an electron paramagnetic resonance (EPR) center has been observed in hBN [41]. The experimental data clearly shows splitting pattern of five peaks with relative intensities of 1:2:3:2:1. This is due to the hyperfine coupling between one electron spin and two equivalent nitrogen nuclear spin of $I = 1$, therefore, the EPR center

has been tentatively associated with the spin doublet of $n-C_N V_B(-)$ defect [41]. Although, our calculations indicate that $n-C_N V_B(-)$ does not exist in hBN, we still simulated its EPR spectrum after calculation of the hyperfine tensors of the defect (see Tab. II). Indeed, the simulated EPR spectrum of $n-C_N V_B(-)$ agrees with the experimental one [41] (Tab. II). We note that the hyperfine signatures of the HSs configuration significantly differ. The stable $sw-C_N V_B(-)$ has very different spin density distribution with localized on two boron ions, thus its EPR spectrum significantly deviates from that of the observed EPR center. However, $n-C_N V_B(-)$ is not a stable structure, therefore, we conclude that it cannot account for the EPR center as tentatively proposed in Ref. [41], despite the agreement between the simulated and observed hyperfine related features in the EPR spectra.

We found that the most stable form of carbon-vacancy complex in hBN is $V_N C_B$ thus, we plot the simulated EPR spectrum for the paramagnetic $V_N C_B(+)$ in Fig. 5(b) which may occur in hBN. The EPR spectrum shows 7 peaks due to two neighboring boron atoms ($I = 3/2$ for ^{11}B). Further experimental data is needed to confirm the existence of such kind of defect.

We note that there is a metastable triplet state for $V_N C_B(0)$. The triplet state may be accessed by optical pumping of the system from the singlet ground state to the singlet excited state followed by an intersystem crossing from the excited singlet state towards the metastable triplet state. However, the large singlet-triplet energy gap makes this process inefficient, thus, we do not consider the triplet of $V_N C_B(0)$ to be observed by photo-EPR studies.

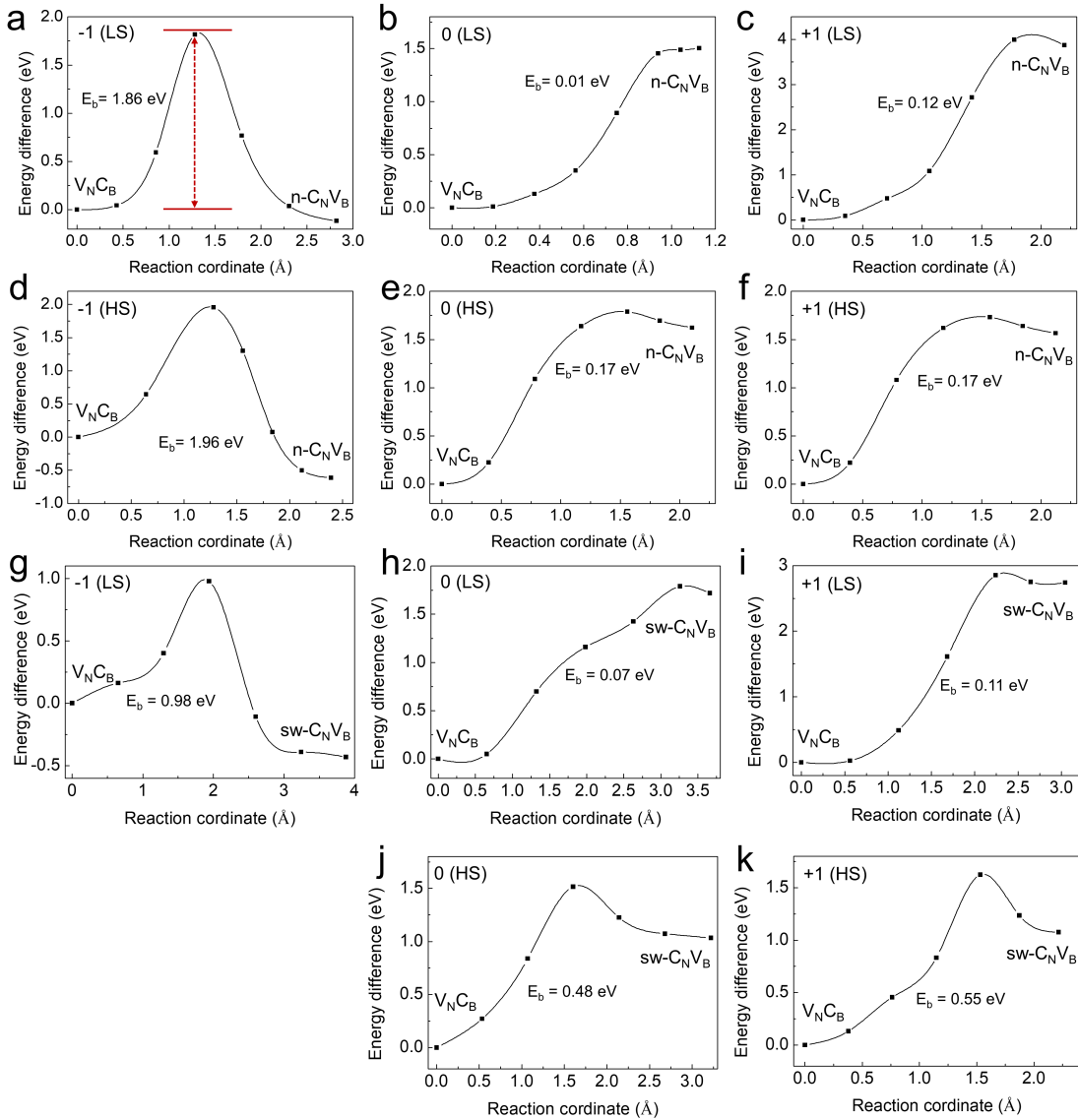


FIG. 4. The reaction barrier for the carbon atom from initial state $V_N C_B$ to final state $C_N V_B$ in different charge states. Transitions from $V_N C_B$ to $n-C_N V_B$ (a-f) and from $V_N C_B$ to $sw-C_N V_B$ (g-k) are shown here. The red arrow indicates the reaction barrier E_b . The HSs of $C_N V_B$ does not have $sw-C_N V_B$ configuration.

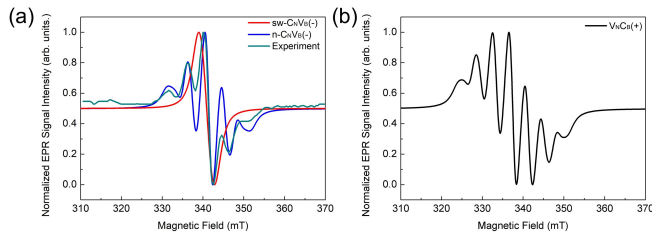


FIG. 5. The simulated EPR spectrum of defects considered. (a) The experimental data is from [41] recorded at 550 °C to clearly show the line splitting. $sw-C_N V_B$ has relative small hyperfine coupling so there is no line splitting. The experimental spectrum is shifted 4 mT towards left to match simulation result. (b) The EPR spectrum of $V_N C_B(+)$.

IV. SUMMARY AND CONCLUSION

In this study, we performed density functional theory calculations on the carbon-vacancy complexes in hBN. The analyzed relative stability of these complexes could reveal the origin of the single photon emitters observed in experiments in the visible wavelength region. $sw-C_N V_B$ is always more stable than $n-C_N V_B$ and $n-C_N V_B$ transforms to $sw-C_N V_B$ without any barrier in three charge states. Hence, previously reported $n-C_N V_B$ is not the origin of visible SPEs in hBN. $sw-C_N V_B$ is metastable and can transform to $V_N C_B$ with some barrier energies depending on the charge states. In addition, neither the $V_N C_B$ nor $C_N V_B$ is a potential candidate for the SPEs associated with the carbon impurities. The formation en-

TABLE I. The lowest vertical transition energy for two defects in hBN. The energy unit is eV. The simulated annealing temperature (temp.) is also listed as obtained from the calculated barrier energies (see text). For $C_N V_B$ defect, except for the $C_N V_B(-)$ HSs, other charge states have lower total energy with sw- $C_N V_B$ configuration. The ΔE_{diff} indicates energy difference between these two configurations and defined as $\Delta E_{diff} = E(n-C_N V_B) - E(sw-C_N V_B)$.

configuration	-1 HS	-1 LS	0 HS	0 LS	+1 HS	+1 LS
$V_N C_B$	0.64	0.87	1.86	1.93	1.81	2.10
SYM.	C_{2v}	C_s	C_{2v}	C_s	C_{2v}	C_{2v}
HR factor			1.50 ^a	7.25		24
n- $C_N V_B$	2.05	1.02	1.75	1.97	0.81	0.91
SYM.	C_{2v}	C_{2v}	C_{2v}	C_{2v}	C_{2v}	C_{2v}
HR factor	2.2					
sw- $C_N V_B$	-	1.12	1.49	2.57	0.14	0.49
ΔE_{diff}	-	0.37	0.70	0.90	2.0	0.78
HR factor				8.17		
TEMP.(K)	705	353	173	25	198	40

a. Simulated data from Ref. [34]

TABLE II. Hyperfine constants for carbon-vacancy complexes in hBN. The unit is in MHz.

	configuration	A_{xx}	A_{yy}	A_{zz}
^{14}N	Exp. [41]	90-98	90-98	145-148
^{14}N	n- $C_N V_B(-)$ LS	86.92	83.12	166.41
^{14}N	n- $C_N V_B(-)$ HS	34.05	33.04	59.54
^{14}N	sw- $C_N V_B(-)$ LS	6.75	6.53	13.25
^{11}B	$V_N C_B(+)$ LS	101.47	100.75	126.87

ergies for $V_N C_B$ and $C_N V_B$ complexes imply that these complexes cannot account for the experiments claiming that the number of C-B bond is larger than C-N bond in carbon contaminated hBN [4]. Further investigation is needed for finding the microscopic origin of SPEs associated with the carbon impurities. Recent studies proposed the $C_2 C_N$ configuration [42–44] of which optical properties well reproduce the experimental data. We also found that the recently reported EPR center [41] is not associated with the unstable $V_N C_B$ defect. Further investigation is needed to identify this EPR center in hBN. We provide the EPR spectrum for the most stable carbon-vacancy complex in hBN that might be found in future EPR studies of carbon contaminated hBN layers.

V. METHODS

We performed spin-polarized DFT calculation within the Kohn-Sham scheme as implemented in the VASP code [45, 46]. Standard projector augmented wave (PAW) formalism [47, 48] is used to separate the valence electrons from nuclei. The convergence threshold is 0.01 eV/Å for force acting on each atoms and energy cut-off for the expansion of the plane-wave basis set is 450 eV. The screened hybrid density functional of Heyd, Scuseria, and Ernzerhof (HSE) [49] is used to calculate the electronic structure and localize bound states. In this approach, we could mix part of nonlocal Hartree-Fock exchange to the generalized gradient approximation of Perdew, Burke, and Ernzerhof (PBE) with fraction α . $\alpha = 0.32$ can reproduce the experimental band gap about 6 eV. We embedded the carbon defects in a $9 \times 5 \sqrt{3}$ monolayer supercell with 162 atoms which is sufficient to avoid the periodic defect-defect interaction, a vacuum layer of 12 Å is applied to separate the periodic layer images. The single Γ -point scheme is converged for the k-point sampling for the Brillouin zone. The excited states were calculated by Δ SCF method [50]. For the formation energy calculation, a bulk model with two hBN layers is used to include the interlayer interaction and decreases the artificial influence induced by vacuum layer. The charge correction term is computed by SXDEFECTALIGN code from Freysoldt method [51]. During the NEB calculation, for $V_N C_B$ to $C_N V_B$ transition, the threshold of force is set to 0.02 eV/Å whereas for n- $C_N V_B$ to sw- $C_N V_B$ transition it is 0.1 eV/Å due to the numerical challenges. The electron paramagnetic resonance (EPR) simulation is performed with EASYSPIN software at X band region (9.45 GHz) [52].

The total HR factor is defined as the number of an effective phonon participating in the optical transition which is a key parameter of the absorption and fluorescence spectra. The total HR factor can be readily calculated within Franck-Condon approximation which assumes that the vibrational modes in the ground and excited states are identical. The associated phonon overlap spectral function can be derived from the overlap between the phonon modes in the electronic ground and excited states [50, 53].

AUTHOR CONTRIBUTION

All authors contributed to the discussion and writing the manuscript. AG led the entire scientific project.

COMPETING INTERESTS

The authors declare that there are no competing interests.

DATA AVAILABILITY

The data that support the findings of this study are available from the corresponding author upon reasonable request.

ACKNOWLEDGMENTS

AG acknowledges the Hungarian NKFIH grant No. KKP129866 of the National Excellence Program of

Quantum-coherent materials project and the support for the Quantum Information National Laboratory from the Ministry of Innovation and Technology of Hungary.

-
- [1] T. T. Tran, K. Bray, M. J. Ford, M. Toth, and I. Aharonovich, *Nature Nanotechnology* **11**, 37 (2016).
- [2] A. Gottscholl, M. Kianinia, V. Soltamov, S. Orlinskii, G. Mamin, C. Bradac, C. Kasper, K. Krambrock, A. Sperlich, M. Toth, *et al.*, *Nature Materials* **19**, 540 (2020).
- [3] N. Chejanovsky, A. Mukherjee, J. Geng, Y.-C. Chen, Y. Kim, A. Denisenko, A. Finkler, T. Taniguchi, K. Watanabe, D. B. R. Dasari, *et al.*, *Nature Materials* **20**, 1079 (2021).
- [4] N. Mendelson, D. Chugh, J. R. Reimers, T. S. Cheng, A. Gottscholl, H. Long, C. J. Mellor, A. Zettl, V. Dyakonov, P. H. Beton, *et al.*, *Nature Materials* **20**, 321 (2021).
- [5] F. Hayee, L. Yu, J. L. Zhang, C. J. Ciccarino, M. Nguyen, A. F. Marshall, I. Aharonovich, J. Vučković, P. Narang, T. F. Heinz, *et al.*, *Nature Materials* **19**, 534 (2020).
- [6] R. Bourrellier, S. Meuret, A. Tararan, O. Stéphan, M. Kociak, L. H. Tizei, and A. Zobelli, *Nano Letters* **16**, 4317 (2016).
- [7] A. Bommer and C. Becher, *Nanophotonics* **8**, 2041 (2019).
- [8] T. T. Tran, C. Elbadawi, D. Totonjian, C. J. Lobo, G. Grosso, H. Moon, D. R. Englund, M. J. Ford, I. Aharonovich, and M. Toth, *ACS Nano* **10**, 7331 (2016).
- [9] G. Grosso, H. Moon, B. Lienhard, S. Ali, D. K. Efetov, M. M. Furchi, P. Jarillo-Herrero, M. J. Ford, I. Aharonovich, and D. Englund, *Nature Communications* **8**, 1 (2017).
- [10] N. Mendelson, M. Doherty, M. Toth, I. Aharonovich, and T. T. Tran, *Advanced Materials* **32**, 1908316 (2020).
- [11] G. Noh, D. Choi, J.-H. Kim, D.-G. Im, Y.-H. Kim, H. Seo, and J. Lee, *Nano Letters* **18**, 4710 (2018).
- [12] T. Vuong, G. Cassaboiss, P. Valvin, A. Ouerghi, Y. Chasagneux, C. Voisin, and B. Gil, *Physical Review Letters* **117**, 097402 (2016).
- [13] X. Du, J. Li, J. Lin, and H. Jiang, *Applied Physics Letters* **106**, 021110 (2015).
- [14] L. Museur, E. Feldbach, and A. Kanaev, *Physical Review B* **78**, 155204 (2008).
- [15] A. Sajid, M. J. Ford, and J. R. Reimers, *Reports on Progress in Physics* **83**, 044501 (2020).
- [16] S. Li, J.-P. Chou, A. Hu, M. B. Plenio, P. Udvarhelyi, G. Thiering, M. Abdi, and A. Gali, *npj Quantum Information* **6**, 1 (2020).
- [17] M. Abdi, J.-P. Chou, A. Gali, and M. B. Plenio, *ACS Photonics* **5**, 1967 (2018).
- [18] V. Ivády, G. Barcza, G. Thiering, S. Li, H. Hamdi, J.-P. Chou, Ö. Legeza, and A. Gali, *npj Computational Materials* **6**, 1 (2020).
- [19] J. R. Reimers, J. Shen, M. Kianinia, C. Bradac, I. Aharonovich, M. J. Ford, and P. Piecuch, *Physical Review B* **102**, 144105 (2020).
- [20] A. Sajid, J. R. Reimers, and M. J. Ford, *Physical Review B* **97**, 064101 (2018).
- [21] R. Wang, J. Yang, X. Wu, and S. Wang, *Nanoscale* **8**, 8210 (2016).
- [22] H. Hamdi, G. Thiering, Z. Bodrog, V. Ivády, and A. Gali, *npj Computational Materials* **6**, 1 (2020).
- [23] C. Jin, F. Lin, K. Suenaga, and S. Iijima, *Physical Review Letters* **102**, 195505 (2009).
- [24] A. Gottscholl, M. Diez, V. Soltamov, C. Kasper, A. Sperlich, M. Kianinia, C. Bradac, I. Aharonovich, and V. Dyakonov, *Science Advances* **7**, eabf3630 (2021).
- [25] W. Liu, Z.-P. Li, Y.-Z. Yang, S. Yu, Y. Meng, Z.-A. Wang, N.-J. Guo, F.-F. Yan, Q. Li, J.-F. Wang, *et al.*, arXiv preprint arXiv:2101.11220 (2021).
- [26] M. Kianinia, S. White, J. E. Froch, C. Bradac, and I. Aharonovich, *ACS Photonics* **7**, 2147 (2020).
- [27] H. L. Stern, Q. Gu, J. Jarman, S. Eizagirre Barker, N. Mendelson, D. Chugh, S. Schott, H. H. Tan, H. Sirringhaus, I. Aharonovich, *et al.*, *Nature communications* **13**, 1 (2022).
- [28] F. Wu, T. J. Smart, J. Xu, and Y. Ping, *Physical Review B* **100**, 081407 (2019).
- [29] L. Weston, D. Wickramaratne, M. Mackoito, A. Alkauskas, and C. Van de Walle, *Physical Review B* **97**, 214104 (2018).
- [30] M. Mackoito-Sinkevičienė, M. Maciaszek, C. G. Van de Walle, and A. Alkauskas, *Applied Physics Letters* **115**, 212101 (2019).
- [31] S. Li, A. Pershin, G. Thiering, P. Udvarhelyi, and A. Gali, *The Journal of Physical Chemistry Letters* **13**, 3150 (2022).
- [32] G. Cheng, Y. Zhang, L. Yan, H. Huang, Q. Huang, Y. Song, Y. Chen, and Z. Tang, *Computational Materials Science* **129**, 247 (2017).
- [33] J. R. Reimers, A. Sajid, R. Kobayashi, and M. J. Ford, *Journal of chemical theory and computation* **14**, 1602 (2018).
- [34] A. Sajid and K. S. Thygesen, *2D Materials* **7**, 031007 (2020).

- [35] M. Maciaszek, L. Razinkovas, and A. Alkauskas, *Physical review materials* **6**, 014005 (2022).
- [36] G. Henkelman, B. P. Uberuaga, and H. Jónsson, *The Journal of Chemical Physics* **113**, 9901 (2000).
- [37] G. Henkelman and H. Jónsson, *The Journal of Chemical Physics* **113**, 9978 (2000).
- [38] R. Geick, C. Perry, and G. Rupprecht, *Physical Review* **146**, 543 (1966).
- [39] A. Janotti and C. G. Van de Walle, *Physical Review B* **76**, 165202 (2007).
- [40] M. A. Ortigoza and S. Stolbov, *Physical Review B* **105**, 165306 (2022).
- [41] J. Toledo and K. Krambrock, *Journal of Physics D: Applied Physics* **54**, 065303 (2020).
- [42] P. Auburger and A. Gali, *Physical Review B* **104**, 075410 (2021).
- [43] K. Li, T. J. Smart, and Y. Ping, *Physical Review Materials* **6**, L042201 (2022).
- [44] O. Golami, K. Sharman, R. Ghobadi, S. C. Wein, H. Zadeh-Haghighi, C. G. da Rocha, D. R. Salahub, and C. Simon, *Physical Review B* **105**, 184101 (2022).
- [45] G. Kresse and J. Furthmüller, *Computational Materials Science* **6**, 15 (1996).
- [46] G. Kresse and J. Furthmüller, *Physical Review B* **54**, 11169 (1996).
- [47] P. E. Blöchl, *Physical Review B* **50**, 17953 (1994).
- [48] G. Kresse and D. Joubert, *Physical Review B* **59**, 1758 (1999).
- [49] J. Heyd, G. E. Scuseria, and M. Ernzerhof, *The Journal of Chemical Physics* **118**, 8207 (2003).
- [50] A. Gali, E. Jánzén, P. Deák, G. Kresse, and E. Kaxiras, *Physical Review Letters* **103**, 186404 (2009).
- [51] C. Freysoldt and J. Neugebauer, *Physical Review B* **97**, 205425 (2018).
- [52] S. Stoll and A. Schweiger, *Journal of magnetic resonance* **178**, 42 (2006).
- [53] A. Alkauskas, B. B. Buckley, D. D. Awschalom, and C. G. Van de Walle, *New Journal of Physics* **16**, 073026 (2014).